Materials and Structures (2022) 55:209
https://doi.org/10.1617/s11527-022-02048-x

ORIGINAL ARTICLE

Nonlinear steel strains in cracked RC beams based on bond-stress profiles

Chunyu Fu · Zhenfeng Gao · Peng Yan

Received: 12 June 2022 / Accepted: 9 September 2022 / Published online: 17 September 2022

Abstract Steel–concrete bond is instrumental in transferring tensile forces to the concrete via the bond stresses, whose values and distribution along a steel bar vary with the level of the load applied to the reinforcement. To study the profile of the strains in the reinforcement, the variation of the bond-stress distribution is considered and the bond stresses are introduced according to Model Code 2010. The transfer length where the bond stresses are active is shown to be a function of the slip in the cracked sections. This slip can be evaluated from the concrete strains based on the plane-section hypothesis to take care of the strain compatibility between the concrete and the reinforcement. The equilibrium of the internal forces, the constitutive laws of the materials and the bond stress-slip law make it possible to model the kinematic interaction between the concrete and the reinforcement. An iterative algorithm is proposed to calculate the steel strains, and the effectiveness of the numerical procedure is checked against the test data coming from simply-supported RC beams tested in this research project or available in the literature. The results show that the nonlinear evolution of steel–concrete slip close to the cracks may increase the transfer length of the bond stresses by 50% under increasing loads, and the steel strains by up to 90% along the bonded length. As a result, the steel-strain profile becomes a slightly-nonlinear function of the load, which is also markedly affected by the crack pattern.

Keywords Cracked RC beams · Steel–concrete bond · Bar slip · Steel strains · Bond–slip law · Bond-related internal forces

1 Introduction

Cracking easily occurs in reinforced concrete beams due to the low tensile strength of the concrete, and causes a slipping between the concrete and the steel bars, to the possible detriment of steel–concrete bond. In cracked sections, bars bear large tensile forces, while the cracked concrete is practically load-free [1]. However, the concrete at a distance from cracked sections still bears some tensile forces because of the force transfer from the bars to the concrete through bond stresses [2]. This phenomenon is known as tension stiffening. The transfer length l_t is defined as an embedment length from the crack to the first point at which the strains of steel and concrete are equal to each other [3], and also can be taken as the active length of the bond stresses.

C. Fu (✉) · Z. Gao
College of Civil and Transportation Engineering, Hohai University, Nanjing, China
e-mail: fuyupiece@163.com

P. Yan
SWJTU Railway Development Co., Ltd., Chengdu, China

Due to tension stiffening, the distribution of the steel strain along the beam axis is not uniform. The strain rises to its maximum in the cracked sections and drops to a minimum at the end of the transfer length [4]. The steel-strain profile is accompanied by a concrete-strain profile, that affects structural stiffness [5] and may impact—even seriously—on structural serviceability and safety. As a result, a model for the steel-strain profile close to the cracks is needed to predict the in-service behavior of RC beams.

Some models for the steel distribution were formulated according to the structural mechanic characteristics near cracks. Kwak et al. [6] directly used a polynomial function to simulate the concrete-strain profile, and adopted the force equilibrium to obtain the steel strains. Xu et al. [7] proposed a method for assessing the overall strains of the steel bars in cracked zones based on the interpolation between the steel strains at concrete cracking and steel yielding. Manfredi et al.[8] assumed that the concrete in compression could be analyzed according to the plane-section hypothesis, and calculated the steel strains based on the concrete compressive strain.

The steel strain may be calculated by integrating the bond stresses and introducing the boundary conditions in the cracked sections. Haskett et al. [9] used a linear bond–slip relationship to formulate a model where the steel strains are a function of crack width. Fayyad et al. [10] adopted this model to analyze the crack propagation of reinforced concrete beams. Yankelevsky et al. [11] assumed a piece-wise linear distribution for the bond stresses, to formulate an incremental model for the steel strains. Wang et al. [12] proposed position functions to modify the bond–slip relationship near cracks, and analyzed the steel-strain profile along the transfer length.

Castel et al. [13] modeled the steel-strain profile between two primary cracks based on a linear distribution of the bond stress, and established a relationship between the steel strains and bending moments. To analyze the effects of internal micro-cracks on the steel strains, a damage variable was introduced by Castel et al. [14] to reduce the bond at the steel–concrete interface during a period of sustained loading. The model was used to calculate the static and dynamic displacements of cracked concrete beams [5, 15].

The above models consider the dependence of the steel strains on steel–concrete slip through bond stresses in cracked reinforced concrete beams, but tend to neglect that the variation in the transfer length of the bond stress, which may cause an underestimate of the steel strains near cracks. In fact, existing experiments of cracked reinforced concrete members had proved that the transfer length was strongly load-dependent [16, 17], so the bond-stress distribution varies with the loads, and the steel strains are affected.

In order to investigate the steel strains, the variation of the bond-stress distribution should be accurately introduced and its effects on the steel strains should be analyzed as well. Therefore, in this paper, the bond stress is derived based on a bond–slip relationship given by Model Code 2010 [18], and its transfer length of the bond stress is shown to change with the slip at the crack, which can be calculated from the concrete strains with the aid of the deformation compatibility of the beam. The steel strains are obtained by integrating the bond stresses, and their effects on the concrete strains are analyzed using the equilibrium of internal forces, so the steel strains and the bond stress interact with each other. An iterative algorithm is adopted to build a solving model for the interaction, and based on the solution, a new method for assessing nonlinear steel strains in cracked RC beams is proposed.

2 Theoretical approach

2.1 Model for steel strains

A reinforced concrete beam with cracks is considered, as shown in Fig. 1, and its depth and width are respectively h and b. An infinitesimal element of a steel bar and its surrounding concrete in the beam is isolated as a free body, as shown in Fig. 2. The steel and concrete strains are defined as $\varepsilon_s(x)$ and $\varepsilon_c(x)$ respectively, where the axial direction of the beam is taken as the x axis. The relationships between the strains and the bond stress τ can be obtained using the force equilibrium conditions.

$$E_s A_s \frac{\mathrm{d}\varepsilon_s}{\mathrm{d}x} = \tau L_s \tag{1}$$

$$E_c A_{ct} \frac{\mathrm{d}\varepsilon_c}{\mathrm{d}x} = \tau L_s \tag{2}$$

where L_s is the contact perimeter of the steel bar with the surrounding concrete, A_s and A_{ct} denote

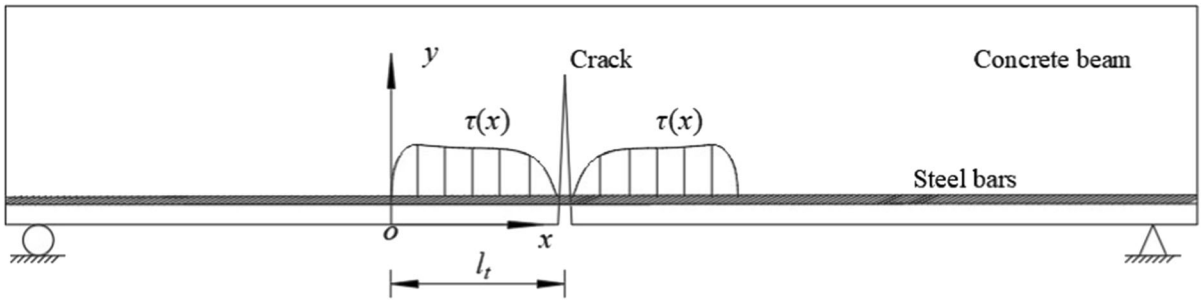

Fig. 1 Bond stress distribution in a cracked RC beam

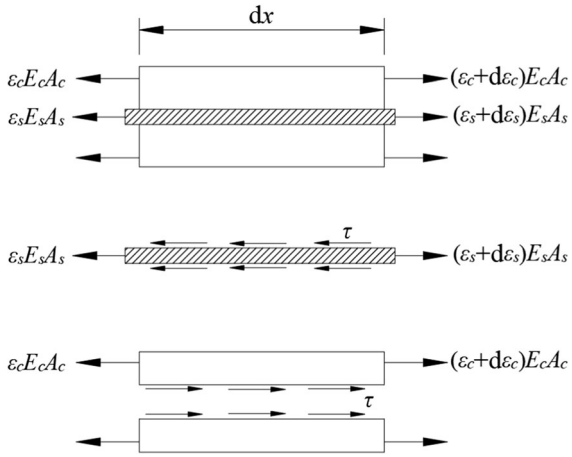

Fig. 2 Strains and stresses in an infinitesimal element

respectively the areas of the steel bar and tensile concrete, and E_s and E_c are their elastic modulus. The slip ds between the steel bar and concrete over a length dx can be regarded as a difference between the strains of the steel bar and concrete

$$\frac{\mathrm{d}s}{\mathrm{d}x} = \varepsilon_s - \varepsilon_c \tag{3}$$

Then through differentiating Eq. (3) with respect to x and substituting Eqs. (1) and (2) into Eq. (3), the following equation is obtained

$$\frac{\mathrm{d}^2 s}{\mathrm{d}x^2} = \tau L_s \left(\frac{1}{E_s A_s} + \frac{1}{E_c A_{ct}}\right) \tag{4}$$

Equation (4) represents the general governing ordinary differential equation defining the bond behavior between the steel bar and concrete [10]. Its solution depends on the function that defines the bond–slip relationship $\tau(s)$. Typical bond–slip relationships were given by Model Code 2010 [18], and based on the behavior of reinforced concrete beams with cracks, the relationship for unconfined concrete whose splitting failure may occur is adopted, as shown in Fig. 3 and Eq. (5).

$$\tau(s) = \begin{cases} \tau_{\max}\left(\dfrac{s}{s_1}\right)^{0.4} & s \le s_1 \\ \dfrac{\tau_{\max}}{s_3 - s_1}(s_3 - s) & s_1 \le s < s_3 \end{cases} \tag{5}$$

where s_1, s_3 and $\tau_{\max}$ are the material coefficients which are determined experimentally and depend on the concrete and steel properties.

By substituting Eq. (5) into Eq. (4), differential equations are obtained

$$\begin{cases} \dfrac{\mathrm{d}^2 s}{\mathrm{d}x^2} - s^{0.4}\beta_1 = 0 & s \le s_1 \\ \dfrac{\mathrm{d}^2 s}{\mathrm{d}x^2} + \beta_2^2 s = \beta_2^2 s_3 & s_1 \le s < s_3 \end{cases} \tag{6}$$

where β_1 and β_2 are calculated coefficients and can be expressed as

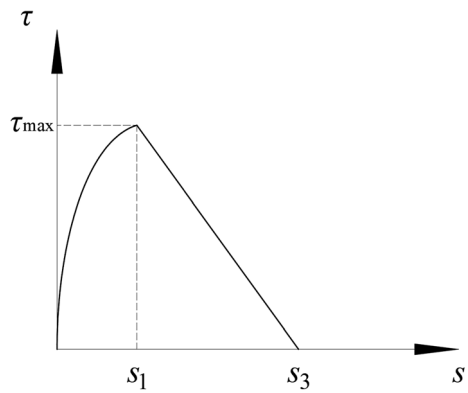

Fig. 3 CEB-FIP bond stress–slip relationship

$$\begin{cases} \beta_1 = \dfrac{\tau_{\max} L_s}{s_1^{0.4}} \left(\dfrac{1}{E_s A_s} + \dfrac{1}{E_c A_c} \right) \\ \beta_2^2 = \dfrac{\tau_{\max} L_s}{(s_3 - s_1)} \left(\dfrac{1}{E_s A_s} + \dfrac{1}{E_c A_c} \right) \end{cases} \tag{7}$$

Assuming the coordinate origin is located at the first point where the steel and concrete strains are equal to each other, as shown in Fig. 1, Eq. (6) can be solved using the boundary condition that $s = 0$ and $\frac{\mathrm{d}s}{\mathrm{d}x} = 0$ at $x = 0$, and the following solution can be obtained

$$s(x) = \begin{cases} \left(\dfrac{10}{7} \beta_1 \right)^{\frac{5}{3}} \left(\dfrac{3}{10} x \right)^{\frac{10}{3}} & s \le s_1 \\ c_1 \cos \beta_2 x + c_2 \sin \beta_2 x + s_3 & s_1 \le s < s_3 \end{cases} \tag{8}$$

where c_1 and c_2 are calculated coefficients, x_1 denotes the x-axis coordinate of the point where the slip is equal to s_1, and they can be expressed as

$$\begin{cases} x_1 = 10 s_1^{0.3} / 3 / \sqrt{10 \beta_1 / 7} \\ c_1 = (s_1 - s_3) \cos \beta_2 x_1 - \left(\dfrac{10}{7} \beta_1 \right)^{\frac{5}{3}} \left(\dfrac{3}{10} x_1 \right)^{\frac{7}{3}} \sin \beta_2 x_1 \\ c_3 = (s_1 - s_3) \sin \beta_2 x_1 + \left(\dfrac{10}{7} \beta_1 \right)^{\frac{5}{3}} \left(\dfrac{3}{10} x_1 \right)^{\frac{7}{3}} \cos \beta_2 x_1 \end{cases} \tag{9}$$

If the slip s along the steel bar is smaller than s_1, by combining Eqs. (1), (5) and Eq. (8) and integrating with respect to x, the tensile force P of the steel bar is calculated.

$$P = E_s A_s \varepsilon_s = E_s A_s \varepsilon_{s0} + \frac{3}{7} \left(\frac{3}{10} \right)^{\frac{4}{3}} \frac{\tau_{\max} L_s}{s_1^{0.4}} \left(\frac{10}{7} \beta_1 \right)^{\frac{2}{3}} x^{\frac{7}{3}} \tag{10}$$

where ε_{s0} is the steel strain at the coordinate origin, and its value is equal to the concrete strain ε_{cs0} at the steel level. So ε_{s0} can be calculated according to the plane-section assumption.

According to Eq. (10), the steel-strain profile in the x-direction and the strain value can be obtained if the coordinate origin is determined. As mentioned above, the coordinate origin is assumed at the first point where the steel and concrete strains are equal to each other, and its distance to the crack is defined as a transfer length l_t, which can be calculated by rewriting Eq. (8) as a function that defines the relationship between l_t and the slip s_c in the cracked section.

$$l_t = \frac{10}{3} \left(\frac{10}{7} \beta_1 \right)^{-\frac{1}{2}} s_c^{\frac{3}{10}} \tag{11}$$

If there is any slip larger than s_1, the tensile force of the steel bar can be obtained by using Eq. (10) for $s < s_1$, and for $s \ge s_1$, its value is calculated by the integrating

$$\begin{aligned} P &= E_s A_s \varepsilon_s \\ &= E_s A_s \varepsilon_{s0} + \frac{3}{7} \left(\frac{3}{10} \right)^{\frac{4}{3}} \frac{\tau_{\max} L_s}{s_1^{0.4}} \left(\frac{10}{7} \beta_1 \right)^{\frac{2}{3}} x_1^{\frac{7}{3}} \\ &\quad + \frac{\tau_{\max} L_s}{\beta_2 (s_3 - s_1)} (-c_1 \sin \beta_2 x + c_2 \cos \beta_2 x) \end{aligned} \tag{12}$$

by rewriting Eq. (8), the transfer length l_t can be expressed as

$$l_t = \frac{1}{\beta_2} \left[\arcsin \left(\frac{s_c - s_3}{\sqrt{c_1^2 + c_2^2}} \right) - \arctan \frac{c_1}{c_2} \right] \tag{13}$$

From Eqs. (11) and (13), it is seen that the transfer length l_t is a variable which varies with the slip s_c in the cracked section. As s_c changes with the load acting on the beam, l_t also varies with the load and the internal force of the beam.

2.2 Calculation of the slip s_c in the cracked sections

The steel bars are subjected to a large tensile force in the cracked sections, while the strains of the concrete near the bars are nearly equal to 0. Therefore, there is a large slip between the steel bars and concrete at the crack. As the slip is directly related to concrete strains, the strain profile should be analyzed.

The concrete strains of the beam bottom are studied firstly. At the coordinate origin, the section is hardly affected by the crack, and its strain profile accords with the plane-section hypothesis, so the bottom strain ε_{cb0} can be obtained by using the classical beam theory

$$\varepsilon_{cb0} = \frac{M_0}{E_c I_0} y_n \tag{14}$$

where y_n is the y-axis coordinate of section neutral axis, I_0 denotes the inertia of sections unaffected by the crack, E_c is the concrete elastic modulus, and M_0 is the section bending moment.

In the cracked sections, however, the strains in the bottom fibers are equal to 0, as crack interfaces are load-free. Therefore, the bottom strains change from ε_{cb0} to 0 along the transfer length. This change can be described by a quadratic polynomial [13], and by using the boundary conditions at the coordinate origin and the crack, the bottom strains ε_{cb} can be written as

$$\varepsilon_{cb}(x) = \left(1 - \frac{x^2}{l_t^2}\right)\varepsilon_{cb0} \quad (0 \le x \le l_t) \tag{15}$$

Then the strain profiles along the depth of sections near the crack are analyzed. Because of cracking, the distribution is no longer linear. A nonlinear model is used to simulate the distribution, as shown in Fig. 4. An inflection point appears at the position whose height is identical with that of the crack tip, because the crack occurrence causes two distinct strain profiles of the parts above and below the tip. The strains of the above part keep linear along the depth, while the strains of the below part follow a nonlinear distribution, which can be expressed as

$$\varepsilon_c(y) = \left(\varepsilon_{ct}\frac{d_c - y_n}{h - y_n} - \varepsilon_{cb}\right)\left(\frac{y}{d_c}\right)^{\eta} + \varepsilon_{cb} \quad y \le d_c \tag{16}$$

where the parameter η denotes the nonlinear distribution, and here is assumed to be related to the rate of σ_{cb0} to σ_{cb} [19].

$$\eta = \mathrm{int}(\varepsilon_{cb0}/2\varepsilon_{cb}) \tag{17}$$

where int() denotes an algorithm that rounds a number to the nearest integer.

The steel bars and concrete are assumed to be elastic, and their stress–strain relationships are linear.

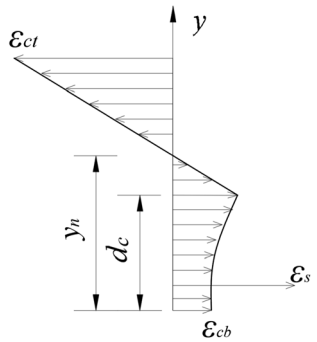

Fig. 4 Strain profile in a cracked section

So the steel stress σ_s and concrete stress σ_c can be written as

$$\sigma_s = E_s\varepsilon_s \tag{18}$$

$$\sigma_c = E_c\varepsilon_c \tag{19}$$

To evaluate the strain in the top fibers of the section and the position of the neutral axis, the internal force equilibria of the sections are used under the bending moment [19, 20].

$$\int_{A_c} \sigma_c(y)\mathrm{d}A + \sigma_s A_s = 0 \tag{20}$$

$$\int_{A_c} \sigma_c(y)(y - y_n)\mathrm{d}A + \sigma_s A_s(d_t - y_n) = M_0 \tag{21}$$

By substituting the steel and concrete strains into Eqs. (18) and (19), the top strain and the neutral axis are determined.

Based on these strain profiles, the slip s_c between the steel and concrete at the crack will be calculated. The slip s_c can be considered as the difference between the deformations of the steel bar and its surrounding concrete, which is expressed as

$$s_c = \Delta l_s - \Delta l_c \tag{22}$$

where Δl_s denotes the elongation of the steel bar, and Δl_c is the deformation of the surrounding concrete. Δl_c can be viewed as the sum of the concrete strain, and written as

$$\Delta l_c = \int_0^{l_t} \varepsilon_{cs}(x)\mathrm{d}x \tag{23}$$

where ε_{cs} is the strain of the surrounding concrete.

The concrete in compression and the bars in tension are continuous across the cracked sections, and their deformations meet the plane-section assumption at the coordinate origin. Furthermore, the deformations are assumed to be symmetric about the crack. Therefore, the steel elongation Δl_s is considered to be compatible with the compression of the beam top concrete over the transfer length, and expressed as a function of the concrete strain ε_{ct} at the top.

$$\Delta l_s = \int_0^{l_t} \frac{\varepsilon_{ct}(x)}{h - y_n(x)}[y_n(x) - d_t]dx \tag{24}$$

Once the slip s_c is determined, the transfer length can be calculated using Eqs. (11) or (13), and the steel strains can be obtained using Eqs. (10) or (12).

2.3 Computational algorithm

The previous analysis allows to conclude that the bond stress affects the steel strain, but its acting length, the transfer length, depends on the steel–concrete slip in the cracked sections according to Eqs. (11) and (13). As the slip can be calculated from the concrete strains, whose values are related to the steel strains based on the internal force equilibria in Eqs. (20) and (21), the steel strains and the bond stress interact with each other. An iterative algorithm is adopted to build a solving model for the interaction and calculate the steel strains:

1. Estimate an initial value of the transfer length l_{tj} ($j = 0$).
2. Use l_{tj} to calculate the steel strains through Eqs. (10) or (12).
3. Select key sections along the transfer length, and calculate their bottom strains using Eq. (15); then build the strain profiles for the sections.
4. Use Eqs. (20) and (21) to calculate the top strains and neutral axes of the sections.
5. Use these top strains and neutral axes to calculate the slip s_c at the crack through Eqs. (22)– (24).
6. Calculate the transfer length $l_{t(j+1)}$ using Eqs. (11) or (13), and by comparing the latest transfer lengths, assess whether they satisfy the equation as follows

$$\left\| l_{t(j+1)} - l_{tj} \right\| < \varepsilon \tag{25}$$

   where ε is the permissible error.
7. If Eq. (25) is valid, the transfer length is equal to l_{tj}, and calculatethe steel strains using Eq. (10) or Eq. (12); otherwise, j is assigned to $j + 1$, and return Step (2) to calculate again.

3 Experimental validation

3.1 Experimental work in this study

Two reinforced concrete beams with simple supports, denoted B1 and B2, were cast by using the same materials. In both cases, the span was 2.6 m and the section rectangular ($b \times h = 200 \times 310$ mm). The main longitudinal steel bars at the bottom of the beams were hot-rolled ribbed bars of 16-mm diameter, and the longitudinal bars at the top and the stirrups were both round bars of 8-mm diameter. The stirrup spacing was 100 mm near the supports, and increased to 150 mm near the midspan. The detailed reinforcement layout of the beams is shown in Fig. 5. The mechanical characteristics of concrete were as follows: mean compressive strength f_{cm} = 38.5 MPa; flexural tensile strength f_{ct} = 2.2 MPa; and elastic modulus E_c = 23 GPa. The elastic modulus E_s and the strength at yielding f_y of the bars were 200 GPa and 400 MPa, respectively.

To record the strain of the longitudinal reinforcement bars, the bars were cut open, slots were milled in the bar interior, and then strain gauges were attached to the inner slots. The size of each gauge was 3.5 mm × 6.5 mm, and the spacing between the adjacent gauges was 20 mm. 30 gauges were attached for each beam, and their distribution is shown in Fig. 6. The central point of the distribution coincided with the beam midspan. To lead out the wires of the gauges, three holes were drilled in the milled zone, and their diameter was 6 mm. After the gauge attachment, epoxy resin was poured into the slots, and the two parts of each bar were pasted together. Then the bars were placed inside the formwork and the concrete was poured.

The test beams had been moist cured for 28 days and then cracked under a precracking loading test. In the precracking loading test, the beams were subjected to a three-point bending load. The peak load was equal to 50kN, and a stabilized cracking pattern was established, which was accurately recorded, as shown in Fig. 7. After concrete cracking, the loading and unloading cycles of four-point bending were performed, as shown in Fig. 5, and the maximum loads in the cycles were not bigger than 64 kN. The loading progress of each cycle is divided into 10 steps, each of which has a same loading increment and a holding time longer than 20 min. The unloading progress of each cycle is divided into 5 steps, each of which has a same holding time with the loading step. Before the start of the cycles, the readings of all the strain gauges were reset to zero, and the steel strains and load values were recorded at each step.

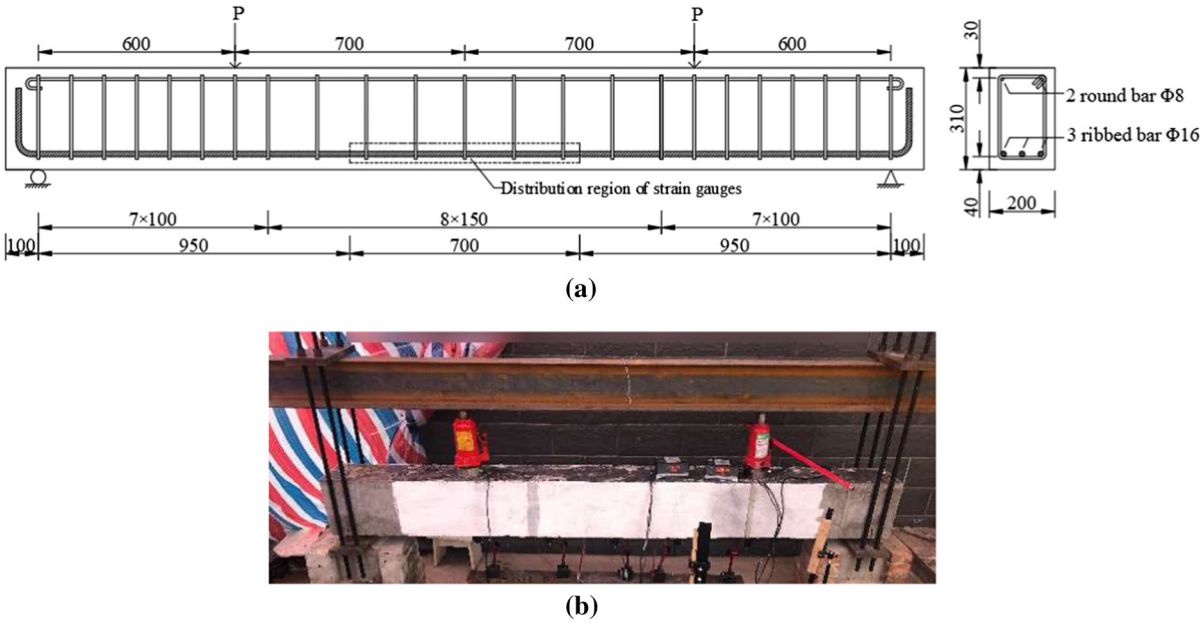

Fig. 5 Geometry of the specimens (**a**) and test setup (**b**) (unit: mm)

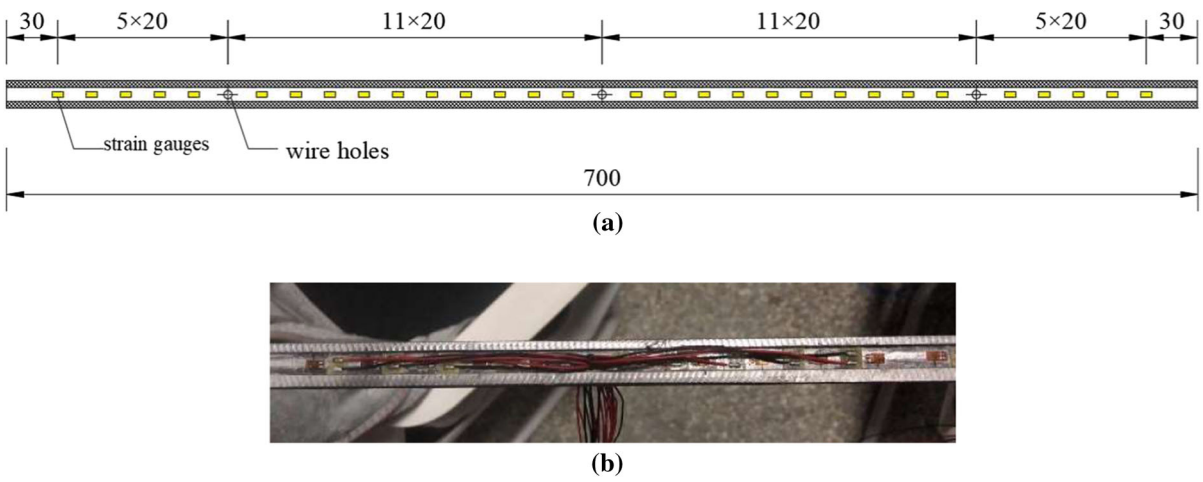

Fig. 6 Distribution of steel strain gauges: **a** size of the gauge distribution region and **b** photo of the attached gauges (unit: mm)

Based on the recorded load, the steel strains and slip in the cracked section are calculated by the proposed method, and the strains are also analyzed using the Castel et al.'s method [13]. The strain results are compared with the recorded data, as shown in Fig. 8 where d_l denotes the distance of the strain gauge to the left end of the beams. It is observed that an acceptable agreement is obtained between the experimental data and the results calculated by the proposed method.

Since the specimens were tested in 4-point bending, the bending moment was constant between the two point-loads and so in the cracked region. In this region, however, the steel strains were not constant in the zone, because of their concentration close to the cracks. From the correlation between the crack location in Fig. 7 and the strain profile in Fig. 8, it is seen that the steel strains reach their maximum at the crack, and over a certain length, reduce to ε_{s0}, whose value is unaffected by the crack and equal to the concrete strain at the steel level.

From Fig. 8, it is also observed that the distribution of the steel strains varies with the loads. At small load

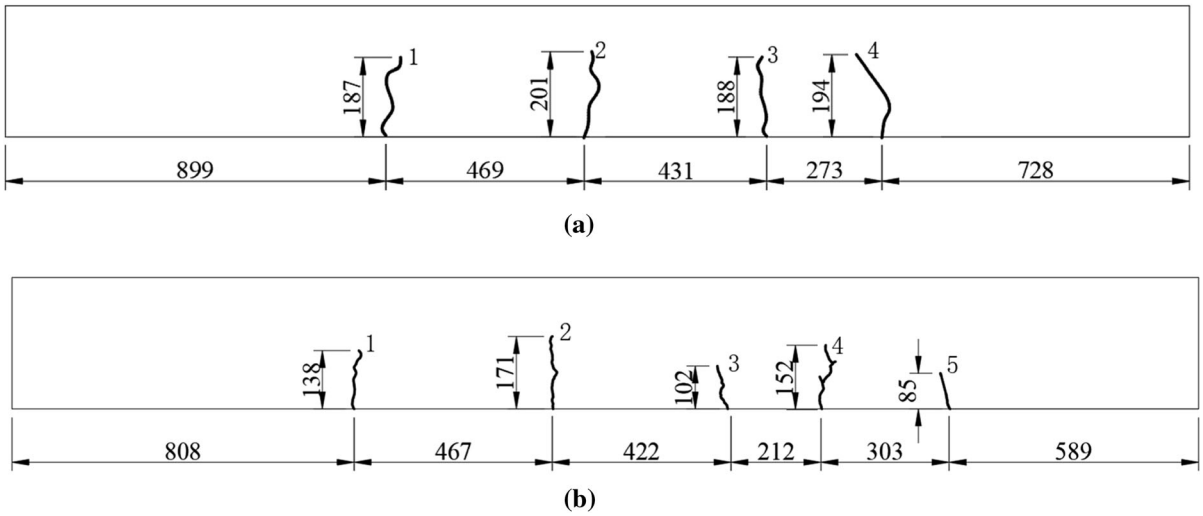

Fig. 7 Crack patterns in **a** the beam B1 and **b** the beam B2 (unit: mm)

levels, the length of the strain change from the maximum to ε_{s0}, also taken as the transfer length, is short, while under the big loads, the length is relatively long. For an example, the length is 50 percent longer under the load of 32kN than under the load of 17kN. It is because the slip s_c at the crack increases with the loads, as shown in Fig. 9, and according to Eq. (10), the transfer length l_t becomes bigger with the increase of s_c.

l_t represents the length of the region whose steel strains are affected by the bond stress and not equal to ε_{s0}, so the change of l_t means the redistribution of the steel strains. Therefore, under the bigger load, there are more gauges whose measured strains are larger than ε_{s0}. For an example, under the load of 32 kN, the steel strain rises by nearly 90% in the position whose d_l is equal to 1.25 m, compared to ε_{s0} whose value is 1.52×10^{-4}. By considering the change of the transfer length, the proposed method can obtain the strain results which are consistent with test data. However, the Castel et al.'s method assumed that the transfer length was constant [13], and its result is still equal to ε_{s0} in this position, as shown in Fig. 8.

Figure 10 shows the effects of load on the steel strains of different positions. The strain changes with the load, but its change rate increases suddenly at some positions when the load reaches a certain value. As the steel bars and concrete are assumed to be elastic in the calculation, the change can be attributed to the fact that the steel–concrete slip varies with the load, as shown in Fig. 9. At small load levels, the slip may not appear, and the steel strains can be calculated based on the plane-section hypothesis, so the change rate of the strains is small. At larger load levels, however, the slip appears at some positions, and causes the steel bars to bear a larger tensile force, thus the change rate becomes larger. For an example, at the position whose d_l is equal to 1.26 m, the rate is about 1.5 times bigger at large load levels than at small load levels.

From Fig. 10, it is also observed that the closer the positions are to the crack, the smaller the loads that change the increase rate of the steel strain are. It is because the slips at the closer positions appear at smaller load levels, which causes the increase rate to become larger. On the contrary, if the position is far enough from the crack, the steel strain is not affected by the crack, and its increase rate will remain constant. Therefore, the steel-strain profile depends on the crack location.

3.2 Validation using experimental data from the literature

A second validation of the proposed model is made using experimental data of reinforced concrete beams cast by Brault and Hoult [21]. The beam LB2c is considered in this study, as the values of the steel strains and the crack patterns are well documented [21]. The beam was simply supported (span = 2.0 m; section $b \times h = 300 \times 200$ mm, Fig. 11). There

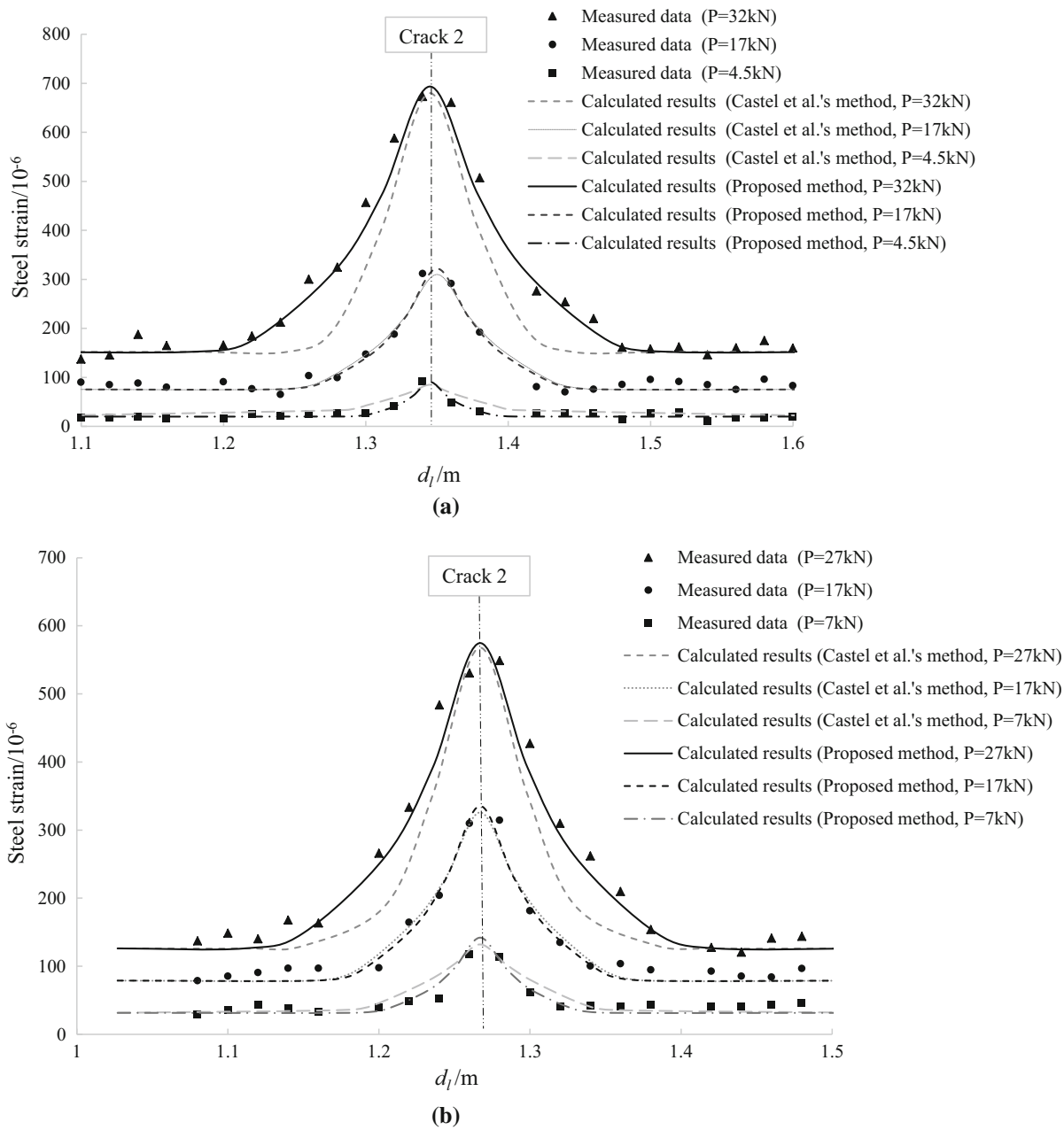

Fig. 8 Profiles of the steel strains astride a crack in **a** the beam B1 and **b** the beam B2

were no stirrup and the longitudinal reinforcement consisted in 15-mm and 10-mm bars, at the bottom and at the top, respectively. The compressive strength of concrete was 29 MPa, and the yield stress and elastic modulus of reinforced steel bars were 445 MPa and 210 GPa, respectively. The distributed steel strains of the beam were measured using fiber optic sensors, which were bonded to the steel surface. The beam was tested in three-point bending until failure using a hydraulic actuator. The load increment of each step was 5kN before cracking, and increased to 10kN after cracking. The crack pattern was recorded during the loading.

According to the recorded data, three cracks, labelled Crack 1, Crack 2, and Crack 3, occurred near midspan, and their distances to the beam's left support

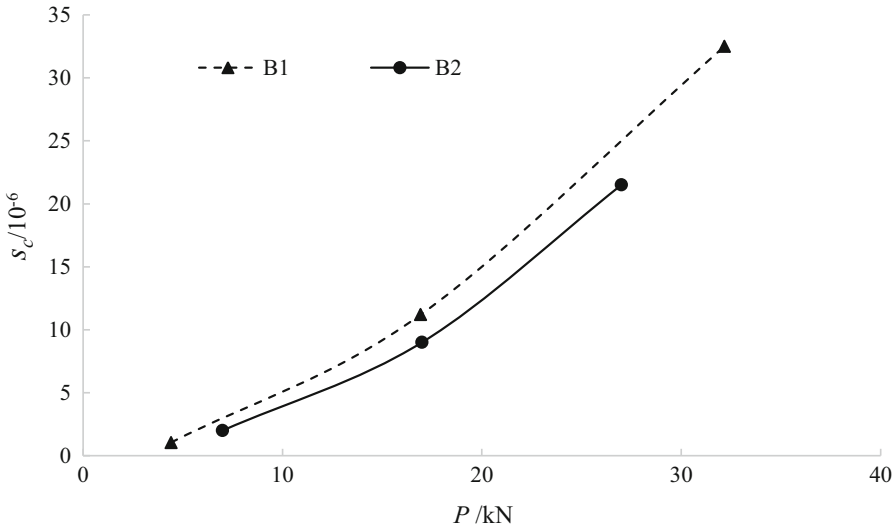

Fig. 9 Slip in the cracked section vs. load

were 0.74 m, 0.95 m, and 1.14 m, respectively. Based on the crack pattern, the steel strains are calculated by means of the proposed model, and compared with the measured steel strains, as shown in Fig. 12. It is observed that the calculated results are close to the experimental data, and have almost the same changing trend as the data.

Under the load of 30kN, the steel strains reach the local maximums at every crack except Crack 1. It is because Crack 1 has not formed, and the slips between the steel bars and concrete do not occur. Thus, the steel strains change linearly with the bending moment near the crack. Under the load of 50 kN, however, Crack 1 is visible and its opening width reaches to 0.24 mm [21]. If the opening width is taken as the slip s_c in the cracked section, the bond stress is large, and the steel strains change greatly near the crack. As a result, the steel-strain profile becomes nonlinear, and its local maximum appears at the crack. Therefore, the steel strains are severely affected by the crack pattern and their nonlinearity becomes obvious at cracks with large opening widths.

4 Conclusions

The following conclusions can be drawn:

1. A method for evaluating the steel strain along the reinforcement in cracked RC beams is proposed by introducing the profile of the bond stress, which plays a major role in the interaction with steel deformability; the equilibrium of the internal forces, the constitutive laws of the materials and the bond stress-slip law make it possible to model the kinematic interaction between the concrete and the reinforcement, which is analyzed by using an iterative algorithm.
2. The effectiveness of the proposed approach has been validated experimentally by testing a number of simply-supported reinforced-concrete beams; the results show that the nonlinear evolution of steel–concrete slip close to the cracks may increase the transfer length of the bond stresses by 50% under increasing loads, and the steel strains by up to 90% along the bonded length.
3. Under increasing loads, the steel strains close to the cracked sections exhibit a nonlinear increase; at small load levels, the slip may not appear and the steel strains are equal to the concrete strains at the steel level, while the steel bars may bear a larger tensile force and the increase rate would be substantial if the load is high enough to cause a steel–concrete slip; the distribution of the steel strains is also markedly affected by the crack pattern associated with the structural shear-bending behavior, as the location and width of the cracks play a substantial role on the magnitude of the slip.
4. The proposed approach can be used to accurately quantify the stress state and the structural behavior of existing reinforced-concrete beams at the Serviceability Limit State; however, the behavior

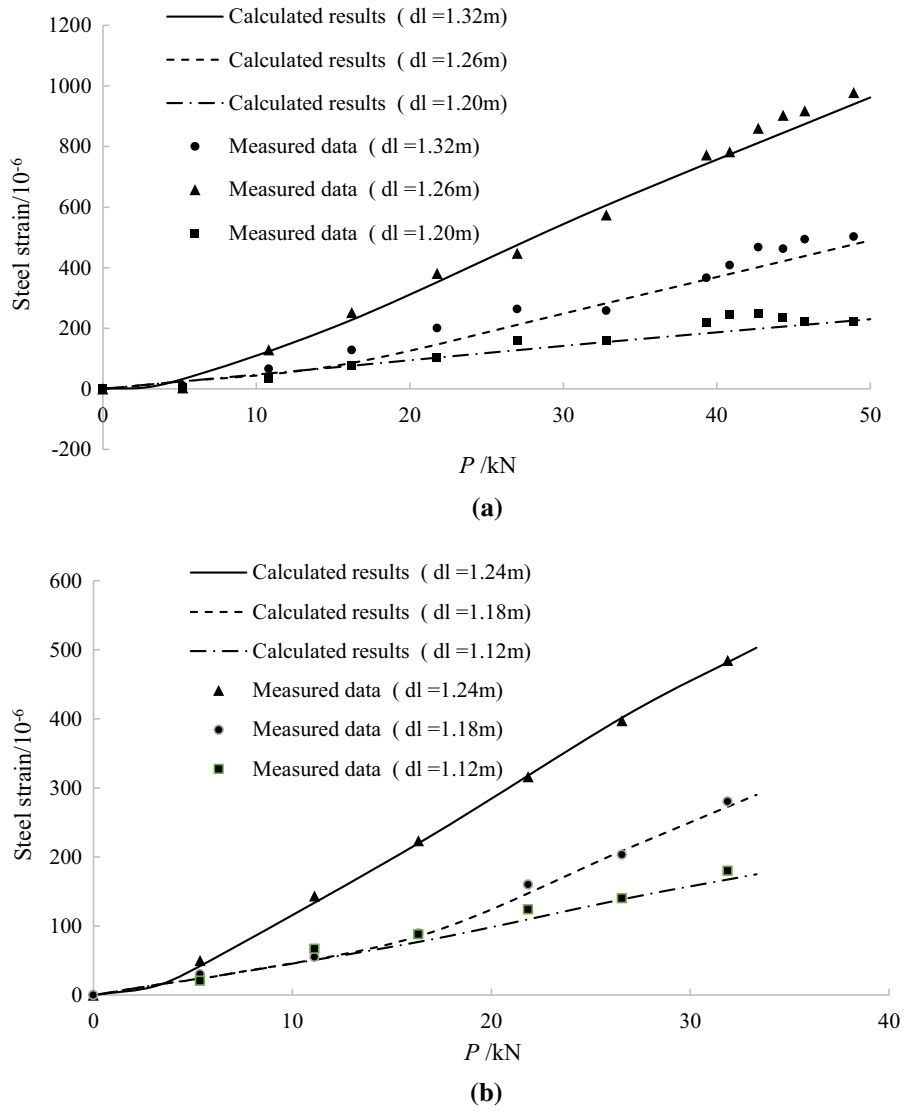

Fig. 10 Steel strain vs. load in the different positions of **a** the beam B1 and **b** the beam B2

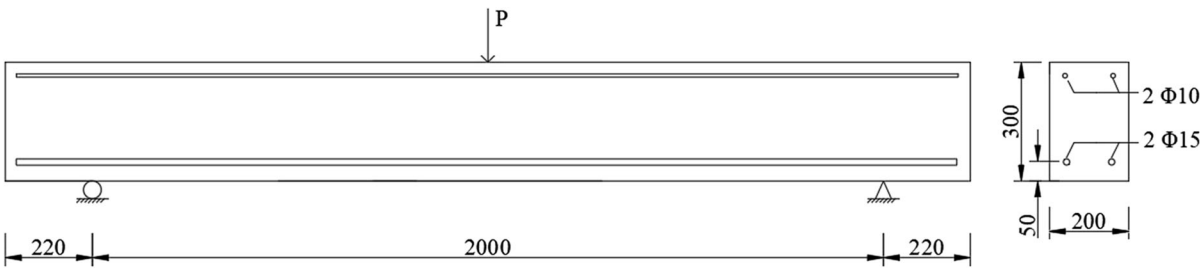

Fig. 11 Geometry of the beam LB2c (unit: mm)

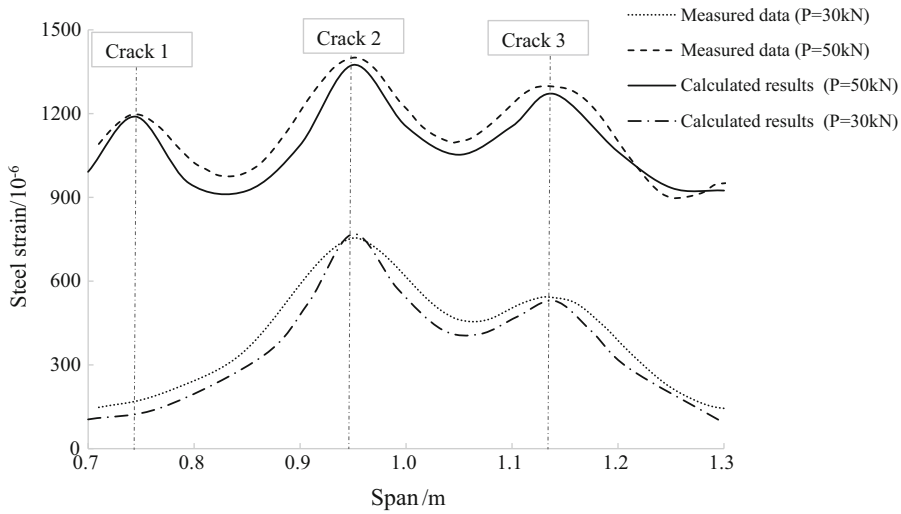

Fig. 12 Beam LB2c: steel–strain profiles under the applied load of 30 kN and 50 kN

may change due to the long-term effect of concrete creep and shrinkage, which is not considered in the proposed approach, so this effect should be investigated in a future study.

Authors' contributions Conceptualization: C.F.; Data curation: Z.G.; Formal analysis: C.F.; Funding acquisition: P.Y.; Investigation: Z.G.; Methodology: C.F.; Project administration: C.F.; Resources: C.F.; Supervision: P.Y.; Validation: Z.G.; Writing—original draft: C.F.; Writing—review & editing: Z.G., P.Y.

Funding This research is sponsored by Science and Technology Project of China State Railway Group Co., Ltd. (N2019G059).

Data availability The research data is available on request from the corresponding author (C.F.).

Code availability Code for data analysis is available on request from the corresponding author (C.F.).

Declarations

Conflict of interest The authors have no conflicts of interest to declare that are relevant to the content of this article.

References

1. François R, Castel A, Vidal T (2006) A finite macro-element for corroded reinforced concrete. Mater Struct 39:571–584
2. Bischoff PH, Paixao R (2004) Tension stiffening and cracking of concrete reinforced with glass fiber reinforced polymer (GFRP) bars. Can J Civil Eng 31(4):579–588
3. Castel A, Vidal T, François R (2012) Finite-element modeling to calculate the overall stiffness of cracked reinforced concrete beams. J Struct Eng 138(7):889–898
4. Murray A, Gilbert RI, Castel A (2018) A new approach to modeling tension stiffening in reinforced concrete. ACI Struct J 115(1):127–137
5. Xu T, Zhu L, Castel A, Gilbert RI (2018) Assessing immediate and time-dependent instantaneous stiffness of cracked reinforced concrete beams using residual cracks. J Struct Eng 144(4):1–12
6. Kwak HG, Song JY (2002) Cracking analysis of RC members using polynomial strain distribution functions. Eng Struct 24(4):455–468
7. Xu T, Castel A, Gilbert RI, Murray A (2016) Modeling the tensile steel reinforcement strain in RC-beams subjected to cycles of loading and unloading. Eng Struct 126:92–105
8. Manfredi G, Pecce M (1998) A refined RC beam element including bond–slip relationship for the analysis of continuous beams. Comput Struct 69:53–62
9. Haskett M, Oehlers DJ, Ali MSM, Wu C (2009) Yield penetration hinge rotation in reinforced concrete beams. J Struct Eng 135(2):130–138
10. Fayyad TM, Lees JM (2018) Integrated fracture-based model formulation for RC crack analysis. J Struct Eng 144(7):04018083

11. Yankelevsky DZ, Jabareen M, Abutbul AD (2011) One-dimensional analysis of tension stiffening in reinforced concrete with discrete cracks. Eng Struct 30:206–217
12. Wang C, Luo F, Cao F, Lu L (2021) Bond–slip behavior and constitutive relation of reinforced and recycled concrete after freezing and thawing. J Build Struct 42(6):214–222
13. Castel A, François R (2011) Modeling of steel and concrete strains between primary cracks for the prediction of cover-controlled cracking in RC-beams. Eng Struct 33:3668–3675
14. Castel A, Gilbert RI, Ranzi G (2014) Instantaneous stiffness of cracked reinforced concrete including steel-concrete interface damage and long-term effects. J Struct Eng 140(6):1–9
15. Vu NA, Castel A, François R (2010) Response of post-tensioned concrete beams with unbonded tendons including serviceability and ultimate state. Eng Struct 32:556–569
16. Murray A, Gilbert RI, Castel A (2018) Spacing of cracks in reinforced concrete based on a variable transfer length model. J Struct Eng 144(7):04018090
17. Turgut C, Jason L, Davenne L (2020) Structural-scale modeling of the active confinement effect in the steel-concrete bond for reinforced concrete structures. Finite Elem Anal Des 172:103386
18. CEB-FIP (2013) Fib model code for concrete structures 2010. Ernst & Sohn, Berlin
19. Fu C, Zhu Y, Tong D (2021) Stiffness assessment of cracked reinforced concrete beams based on a fictitious crack model. KSCE J Civ Eng 25:516–528
20. Fu C, Zhu Y, Wang Y (2020) Stiffness assessment of cracked post-tensioned concrete beams with unbonded tendons based on the cracking pattern. Eng Struct 214:110599
21. Brault A, Hoult NA (2019) Distributed reinforcement strains: measurement and application. ACI Struct J 116(4):115–127